Spectral Induced Polarization applied at different mountain permafrost sites in the European Alps

Introduction

Ground ice content is a key parameter to understand the current state of mountain permafrost and varies from 0 to 100% for different permafrost landforms (e.g. Kenner et al., 2019). Electrical methods have emerged as well-suited to support borehole data and investigate the spatial distribution and temporal evolution of subsurface permafrost characteristics (Hauck et al., 2011), since the electrical properties are sensitive to the phase change from liquid to frozen water in the pore space. Recent laboratory and field studies have investigated not only the conductive but also the capacitive properties of soils and rocks under freezing conditions by means of induced polarization (IP) measurements (Grimm and Stillman, 2015; Doetsch et al., 2015; Duvillard et al., 2018; Coperey et al., 2019). These studies indicate the potential of the frequency dependence of the IP method, the so-called spectral IP (SIP) to quantify ice content (Grimm and Stillman, 2015). In the laboratory, the frequency-dependence has been investigated in details, but so far only few studies applied the IP method in mountain permafrost regions (Duvillard et al., 2018).

Frequency-domain SIP imaging data sets permit to assess the frequency-dependence in the electrical properties directly from the readings, without adding uncertainties due to the inversion. Accordingly, in this abstract we mainly focus on the raw signatures for imaging data sets collected at different sites. We present here SIP results conducted in the frequency range between 0.1-225 Hz at 11 representative morphologically different mountain permafrost sites in the European Alps. The selected study areas range from rock glaciers and talus slopes with high ice contents to bedrock permafrost with lower ice contents. All SIP study sites are located at elevations around 2600 - 3500 m and provide comprehensive geophysical and temperature data for validation.

Methods

The chosen permafrost sites are located in Switzerland, Austria, Italy and Germany, and are presented in Figure 1. The sites include the talus slopes Lapires (LAH) and Dreveneuse (DRE); bedrock permafrost sites in Schilthorn (SCH), Sonnblick (SON), Cervinia Cime Bianche (CER), Lambronecca (LBR), Zugspitze (ZUG), Stockhorn (STO); and the rock glaciers Murtel Corvatsch (MCO), Murtel Baby rock glacier (MBR) and Cervinia Gran Sometta (CGS). Borehole temperature data and ice content information from drilling and complementary geophysical data are used for validation and are available for all sites except for the sites MBR and LBR. Frequency-domain IP (FDIP) data were collected within a frequency range of 0.1-225 Hz using the eight-channel DAS-1 system (from Multi-Phase Technologies) at the 11 sites with the measurement settings summarized in Figure 1. The SIP data presented in this study were acquired with both dipole-dipole (DD) and multiple gradient (MG) configurations, with DD permitting the collection of normal and reciprocal readings for the quantification of data error (e.g. Flores-Orozco et al., 2012); while MG readings were collected due to their high S/N. We note here that in a few sites DD data sets were too noisy and in such cases we only present the MG data. In most of the sites (except MCO and MBR) we deployed coaxial cables to reduce electromagnetic (EM) coupling at higher frequencies (measuring methodology proposed in Maierhofer et al. (2021 in prep.)). The position of the profiles was chosen in close proximity to the available boreholes and the selection of electrode separation aimed at resolving the interface between active layer and permafrost body.

Results

Figure 2 presents the pseudosections for data collected with DD and MG configurations in terms of the apparent resistivity (ρ_{app}) and phase (ϕ_{app}), after removal of outliers following the procedure described in Maierhofer et al. (2021, in prep.). Data quality is evaluated by analysing the misfit of normal and reciprocal readings.

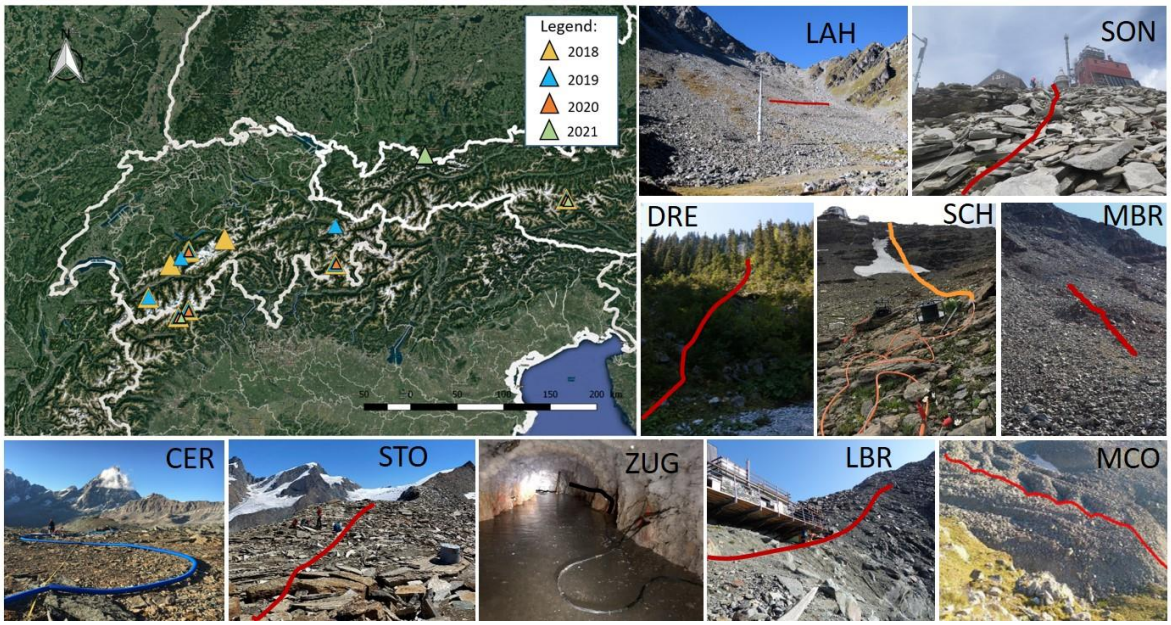

study site	measure-ment date	number of electrodes	electrode spacing (m)	cable type	electrode config	number of quadrupoles
LAH	08/2019	32	5	coaxial	DDsk3 N&R	552
SON	10/2019	32	2	coaxial	DDsk3 N&R	552
DRE	09/2020	32	2	coaxial	MGsk0,3	528
SCH	08/2019	78	10	coaxial	DDsk3 N&R	1656
MBR	08/2018	48	3	multicore	DDsk3 N&R	1518
CER	10/2019	64	3	coaxial	DDsk3 N&R	2947
STO	09/2020	64	2	coaxial	MGsk0,3	744
ZUG	03/2021	42	1.5	coaxial	MGsk0,3	576
LBR	09/2020	32	2	coaxial	DDsk3 N&R	552
MCO	08/2018	48	5	multicore	DDsk3 N&R	1915
CGS	07/2019	64	5	coaxial	MGsk0,3	512

Figure 1 *Overview of the mountain permafrost sites located in the Swiss-, Austrian-, Italian and German- Alps (top) and the measurement setup deployed at 11 mountain permafrost sites*

Pseudosections are shown for ρ_{app} at 0.5 Hz as we observed no frequency-dependence for the magnitude; while ϕ_{app} readings are presented at two frequencies (1 Hz and 75 Hz). Pseudosections allow for an easy visualization of the spatial consistency in the readings and to compare the range of apparent resistivity and phase values measured at the different permafrost sites. Figure 2 reveals the highest ρ_{app} values for MCO, SON and ZUG with mean apparent resistivities between 10^4 and 10^6 Ωm, medium ρ_{app} values for LAH, MBR, STO, CER, LBR, DRE and CGS (with mean apparent resistivities between 10^3 and 10^4 Ωm) and the lowest ρ_{app} observed for SCH (~10^3 Ωm). Mean $-\phi_{app}$ at 1 Hz are highest for MCO (115 mrad) and lowest for SCH (10 mrad). Figure 2 evidences a significant increase in the phase readings for high frequencies (i.e., 75 Hz) when compared to the low frequencies (e.g., 1 Hz). The use of coaxial cables and the general high resistivities of the sites render EM inductive coupling negligible, thus, we argue that the increase in the phase for higher frequencies may be related to the polarization of ice (e.g Grimm and Stillman, 2015). However, the effect of the high resistivity and possible capacitive coupling cannot be completely disregarded.

In Figure 3 we look at the frequency-dependence in the electrical impedance, expressed in terms of ρ_{app} and ϕ_{app}. The ice content values shown in Figure 3 are estimated from borehole information and petrophysical modelling (Mollaret et al., 2020; Steiner et al., 2021). We opted for a comparison of four selected sites representing examples for permafrost conditions with high and low ice content. As

expected for the investigated frequency range, we do not observe a frequency-dependence for ρ_{app} and the values differ by an order of magnitude between LAH 30 % ice content) and SCH (5 % ice content).

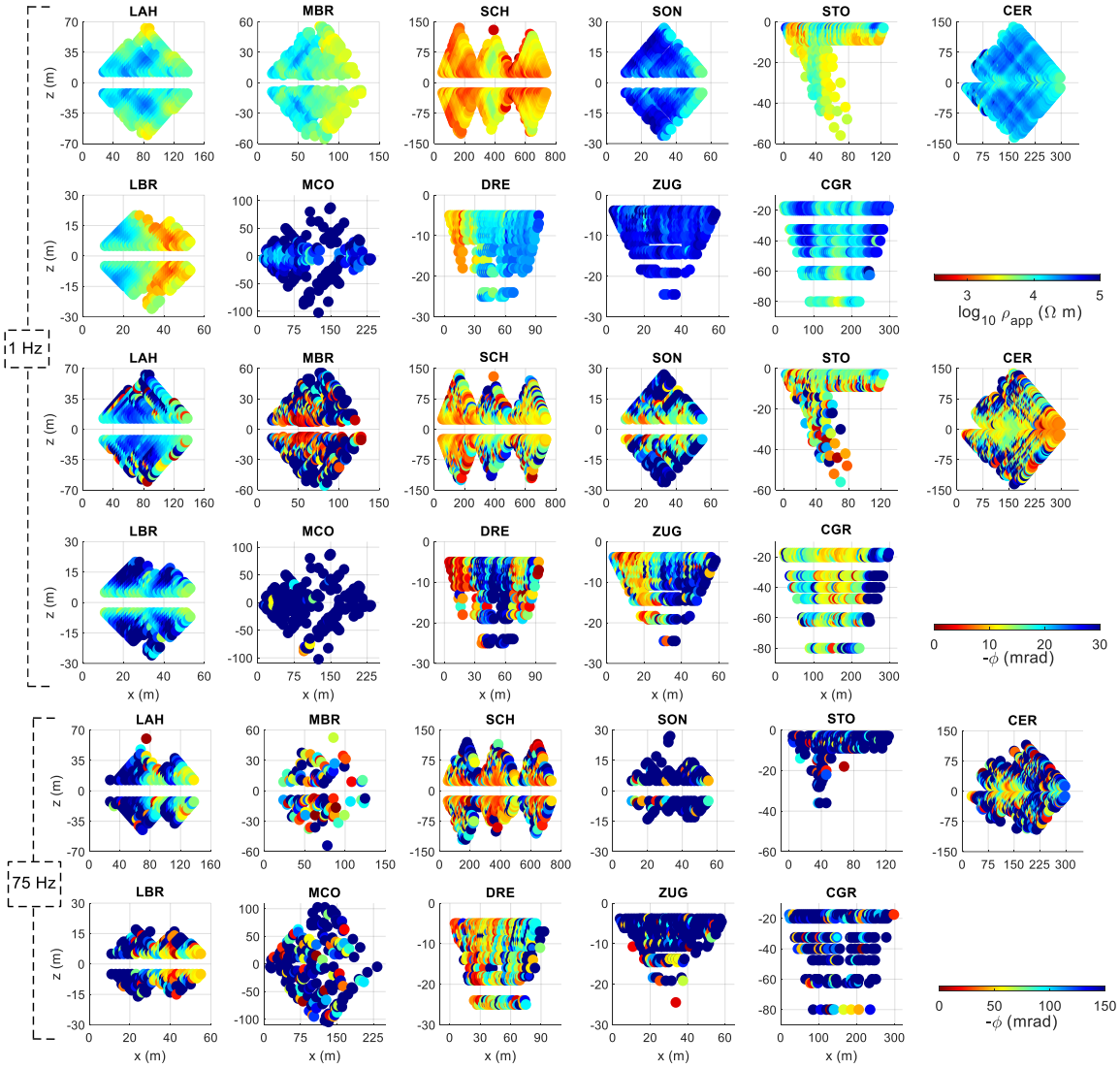

Figure 2 *Pseudosections for SIP data collected at 11 permafrost sites. Pseudosections are presented in terms of the apparent resistivity and phase at 0.5 Hz and 75 Hz.*

We observe similar apparent resistivity values for LAH, CER and DRE; which, however, exhibit completely different ice contents. Likewise, the increase of ϕ_{app} of the electrical impedance at high frequencies (above 10 Hz) seems to reflect a dependence on the ice content. Above 10 Hz, we observe the lowest ϕ_{app} values for the two sites (SCH and DRE) with the lowest ice contents and the highest phase values for the site (LAH) with the highest ice content. Yet, although the results look promising, we need to properly understand the correlation between the phase and the ice content for all different sites.

Conclusions

Our results demonstrate the potential of SIP data, in particular the frequency-dependence of the electrical impedance, to discriminate between alpine permafrost areas with high, medium and low ice content; thus, permitting to improve the interpretation over investigations conducted only with ERT. We show that the polarization is different for ice-rich and ice-poor permafrost sites and that the increase in the ϕ_{app} at high frequencies (> 10 Hz) correlates with an increase in ice content. During the

presentation, we will compare SIP imaging results with available ice content data through borehole data and complementary geophysical information at all sites (Mollaret et al., 2020; Steiner et al., 2021).

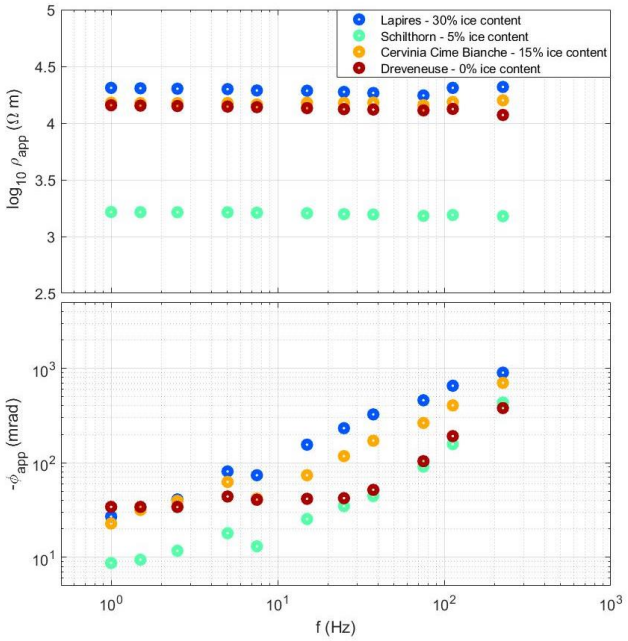

Figure 3 *Visualization of the frequency-dependence in the electrical impedance depicted for representative frozen zones in the pseudosection of 4 permafrost sites with different ice contents.*

References

Coperey, A., Revil, A., Abdulsamad, F., Stutz, B., Duvillard, P. A., and Ravanel, L. [2019]. Low-Frequency Induced Polarization of Porous Media Undergoing Freezing: Preliminary Observations and Modeling. In Journal of Geophysical Research: Solid Earth. https://doi.org/10.1029/2018JB017015

Doetsch, J., Fiandaca, G., Ingeman-Nielsen, T., Fiandaca, G., Christiansen, A. V., Auken, E., and Elberling, B. [2015]. Direct current (DC) resistivity and induced polarization (IP) monitoring of active layer dynamics at high temporal resol. Near Surface Geoscience 2015 - 21st European Meeting of Environmental and Engineering Geophysics, 119, 291–295. https://doi.org/10.1016/j.coldregions.2015.07.002

Duvillard, P. A., Revil, A., Qi, Y., Soueid Ahmed, A., Coperey, A., and Ravanel, L. [2018]. Three-Dimensional Electrical Conductivity and Induced Polarization Tomography of a Rock Glacier. Journal of Geophysical Research: Solid Earth, 123(11), 9528–9554. https://doi.org/10.1029/2018JB015965

Flores-Orozco, A., Kemna, A., and Zimmermann, E. [2012]. Data error quantification in spectral induced polarization imaging. Geophysics, 77(3). https://doi.org/10.1190/geo2010-0194.1

Grimm, R. E., and Stillman, D. E. [2015]. Field test of detection and characterisation of subsurface ice using broadband spectral-induced polarisation. Permafrost and Periglacial Processes, 26(1), 28–38. https://doi.org/10.1002/ppp.1833

Hauck, C., Böttcher, M., and Maurer, H. [2011]. A new model for estimating subsurface ice content based on combined electrical and seismic data sets. Cryosphere, 5(2), 453–468. https://doi.org/10.5194/tc-5-453-2011

Kenner, R., Noetzli, J., Hoelzle, M., Raetzo, H., and Phillips, M. [2019]. Distinguishing ice-rich and ice-poor permafrost to map ground temperatures and ground ice occurrence in the Swiss Alps. 1925–1941.

Mollaret, C., Wagner, F. M., Hilbich, C., Scapozza, C., and Hauck, C. [2020]. Petrophysical Joint Inversion Applied to Alpine Permafrost Field Sites to Image Subsurface Ice, Water, Air, and Rock Contents. 8(April). https://doi.org/10.3389/feart.2020.00085

Steiner, M., Wagner, F. M., Maierhofer, T., Schöner, W., and Flores Orozco, A. [2021]. Improved estimation of ice and water contents in Alpine permafrost through constrained petrophysical joint inversion: The Hoher Sonnblick case study. Geophysics, 1–84. https://doi.org/10.1190/geo2020-0592.